Heat Mass Transfer (2015) 51:1461–1473
DOI 10.1007/s00231-015-1513-7

ORIGINAL

Thermal characteristics of time-periodic electroosmotic flow in a circular microchannel

Ali Jabari Moghadam

Received: 13 February 2014 / Accepted: 4 February 2015 / Published online: 12 February 2015

Abstract A theoretical analysis is performed to explore the thermal characteristics of electroosmotic flow in a circular microchannel under an alternating electric field. An analytical approach is presented to solve energy equation, and then, the exact solution of temperature profiles is obtained by using the Green's function method. This study reveals that the temperature field repeats itself for each half-period. Frequency has a strong influence on the thermal behavior of the flow field. For small values of the dimensionless frequency (small channel size, large kinematic viscosity, or small frequency), the advection mechanism is dominant in the whole domain and the resultant heating (Joule heating and wall heat flux) can be transferred by the complete flow field in the axial direction; while, the middle portion of the flow field at high dimensionless frequencies does not have sufficient time to transfer heat by advection, and the bulk fluid temperature, especially in heating, may consequently become greater than the wall temperature. In a particular instance of cooling mode, a constant surface temperature case is temporarily occurred in which the axial temperature gradient will be zero. For relatively high frequencies, the unsteady bulk fluid temperature in some radial positions at some moments may be equal to the wall temperature; hence instantaneous cylindrical surfaces with zero radial heat flux may occur over a period of time. Depending on the value and sign of the thermal scale ratio, the quasi-steady-state Nusselt number (time-averaged at one period) approaches a specific value as the electrokinetic radius becomes infinity.

A. J. Moghadam (✉)
Department of Mechanical Engineering, Shahrood University of Technology, P.O. Box 316, Shahrood, Iran
e-mail: jm.ali.project@gmail.com

List of symbols

A_c	Cross-sectional area of the channel (m^2)
c_p	Specific heat (J/kg K)
e	Electron charge (C)
E_z	Electrical field strength along axial direction (V/m)
k_B	Boltzmann constant (J/K)
k_{th}	Fluid thermal conductivity (W/m K)
n_0	Bulk ion concentration (m^{-3})
Nu	Mean-time Nusselt number
G_s	Thermal scale ratio
Pr	Prandtl number
q''_s	Imposed constant wall heat flux (W/m^2)
r	Radial coordinate (m)
$\Re$	Radius of the micro-channel (m)
R	Dimensionless radial coordinate
t	Time (s)
T	Absolute temperature (K)
T_s	Local wall temperature (K)
V	Dimensionless axial velocity
V_z	Axial velocity (m/s)
z	Axial coordinate (m)
$\mathbb{Z}$	Valence of ionic species

Greek symbols

χ	The length scale ratio or the electrokinetic radius (ratio of half channel diameter to Debye length)
ε	Electric permittivity of solution (F/m)
Φ	Dimensionless temperature
κ	Debye–Hückel parameter (m^{-1})
μ	Dynamic viscosity (Pa s)
θ	Dimensionless time
ρ	Fluid density (kg/m^3)
σ	Fluid electrical conductivity (S/m)
ω	Frequency (s^{-1})
Ω	Dimensionless frequency

ψ Electrical potential (V)
Ψ Dimensionless electrical potential
ζ Zeta potential at the wall (V)

Subscript
m ≡Mean value

1 Introduction

When the motions of liquids or the solutes are controlled electrically (e.g. in many lab-on-a-chip applications), electrohydrodynamics (EHD) will be the main subject of study. This topic introduces the electric body force into the Navier–Stokes equation for a liquid with a non-zero charge density in an external electric field. If an electrolyte, i.e. an aqueous solution of ions, is in contact with a solid surface (for example, the microchannel walls), depending on the chemical composition of the solid and of the electrolyte chemical processes at the surface will result in a charge transfer between the electrolyte and the wall. As a result, the wall and the electrolyte get oppositely charged, while maintaining global charge neutrality. The ions having the opposite charge of the solid, the counterions, are attracted to the solid, while the other ions, the coions, are repelled. The first layer, known as Stern layer, is a molecular film of counterions which are fixed at the level of the solid/liquid interface under the effect of attractive forces developed by the charged solid surface. The Stern layer is bonded to the solid by an electrostatic interaction. The second layer, named as diffuse layer, is not bonded to the crystalline network (ordered or disordered) of the solid. The structure of diffuse layer results from a statistical equilibrium between thermal agitation (which tends to homogenize the charge distribution) and electrical forces (which tend to displace charges of the same sign towards the surface, thus breaking the homogeneity). The characteristic length scale of this phenomenon, the Debye length, is of order of few nanometers. The potential and the charge density become nearly zero once the distance to the surface is longer than one Debye length. Electroosmotic flow (EOF) is produced when an electric field is applied parallel to the surfaces in the presence of an established double layer. In such a situation, the double layer is moved by the effect of Coulomb forces, and then the rest of the fluid is pulled with it due to viscous forces. Microfluidics is defined as the study of flows (simple or complex, mono- or multiphasic) which are circulating in artificial microsystems. In recent years, there has been a rapid growth in the development of Micro-Electro-Mechanical Systems (MEMS) related devices that pertains to the miniaturization of all kinds of systems. There are several advantages of scaling down standard laboratory setups by a factor of 1000 or more from the decimeter scale to the 100 micro meters scale. One obvious advantage is the dramatic reduction in the amount of required sample. Moreover, the small volumes make it possible to develop compact and portable systems that might ease the use of bio/chemical handling and analysis systems tremendously. Finally, it is the hope by mass production to manufacture very cheap lab-on-a-chip systems that can really be thought of as the shrinking of an entire laboratory to a chip. A lab-on-a-chip device is a miniaturized system including microchannels, electrodes, sensors and electric circuits. Applying electric field along a microchannel also causes a phenomenon named Joule heating that is due to electrical resistivity of the electrolyte. EOF requires electrodes in contact with an electrolyte where an ion current is created. The power needed to drive this ion current is eventually dissipated into heat, and it turns out that this Joule heating usually creates a much more significant temperature shift in the fluid than viscous heating. The electric field strength is limited by Joule heating, due to the electric current crossing the solution containing ions. Although high voltages are often necessary in the EOF, the required electrical power is very small due to the very low current involved. However, heat generated in EOF eventually brings problems to many applications where solutions of high electrolyte concentrations and long operation time are required. Most of electrokinetic processes include pumping, mixing, thermal cycling, dispensing and separating. Understanding of the fluid flow and heat transfer characteristics in microchannels is essential to optimal design and precise operation of microfluidic systems. Another application of microfluidics is in microelectronic engineering in which the electronic cooling of compact and micro-sized circuits is of general interest [1–3].

Extensive studies have been conducted to explore the behaviors of electroosmotic flow in micro-scale devices. Arulanandam and Li [4] studied the liquid movement in a rectangular microchannel by electroosmotic pumping. They used the 2D Poisson-Boltzmann equation and the 2D momentum equation to model the problem. The flow field and volumetric flow rate were presented as functions of the zeta potential, the ionic concentration, the aspect ratio, and the applied electrical field. Erickson and Li [5] presented a combined theoretical and numerical approach to investigate the time-periodic electroosmotic flow in a rectangular microchannel. Kang et al. [6] solved the EOF problem in a cylindrical channel for only sinusoidal waveform by the Green's function method. Tang et al. [7] investigated the electroosmotic flow in axisymmetric microducts. They presented axisymmetric lattice Boltzmann models to solve the electric potential distribution and the velocity field. Wang and Kang [8] presented a numerical solution based on coupled lattice Boltzmann methods for electro-kinetic flows in microchannels. Xuan and Li [9]

used a semi-analytical approach to investigate electroosmotic flows in microchannels with arbitrary cross-sectional geometry and distribution of wall charge. Moghadam [10] obtained the exact solution of the velocity distribution for alternating current electroosmotic flows in a circular microchannel by using the Green's function approach. Oddy et al. [11] proposed and experimentally demonstrated a series of schemes for enhanced species mixing in microfluidic devices using AC electric fields. They also presented an analytical flow field model, based on a surface slip condition approach, for an axially applied AC electrical field in an infinitely wide microchannel. Comprehensive models for a slit channel have also been presented by Dutta and Beskok [12] who developed an analytical model for an applied sinusoidal electric field, and Soderman and Jonsson [13] who examined the transient flow field caused by a series of different pulse designs. Green et al. [14] experimentally observed peak flow velocities on the order of hundreds of micrometers per second near a set of parallel electrodes subject to two AC fields, 180 degrees out-of-phase with each other. The effect was subsequently modeled using a linear double layer analysis by Gonzalez et al. [15]. Using a similar principal, both Brown et al. [16] and Studer et al. [17] presented microfluidic devices that incorporated arrays of non-uniformly sized embedded electrodes which, when subject to an AC field, were able to generate a bulk fluid motion. The time-periodic EOF in a microannulus was investigated by Moghadam [18, 19], in which, the exact solution of velocity distributions has been obtained by the Green's function method. The effects of various periodic waveforms have been also studied.

Soong and Wang [20] studied flow and heat transfer between two parallel plates. The effects of the EDL near the solid–liquid interface and the flow-induced electrokinetic field on the pressure-driven flow and heat transfer through a rectangular microchannel were reported by Yang et al. [21]. Thermally fully-developed, electroosmotically generated convective transport has been analyzed by Maynes and Webb [22] for a parallel plate microchannel and circular microtube. They presented analytical expressions for the fully-developed, dimensionless temperature profile and corresponding Nusselt number for both geometric shapes. Chen [23] investigated thermal transport characteristics of combined electroosmotic and pressure-driven flow in parallel plate channels subject to constant surface heat flux. Analytical solutions were obtained for constant fluid properties, while numerical solutions were presented for variable fluid properties. Sadeghi and Saidi [24] considered the influence of viscous dissipation on thermal transport characteristics of the fully-developed, combined pressure and electroosmotically-driven flow in parallel plate microchannels subject to uniform wall heat flux. Electroosmotic flow and developing heat transfer is analytically studied by Moghadam [25]. Maynes and Webb [26] investigated the influence of viscous dissipation on thermally fully-developed, electroosmotically generated flow in a parallel plate microchannel and circular microtube under imposed constant wall heat flux and constant wall temperature boundary conditions. They examined the effects of governing parameters on the relative magnitudes of total volumetric generation by viscous and Joule heating. Moghadam [27] presented an analytical approach to study the transport characteristics of electroosmotic flow and heat transfer of non-Newtonian power-law fluids in a circular microchannel.

The theory of thermal transfer in microfluidic systems is complex; especially when the alternating electric field is applied. In this research, we pay attention to the thermal behavior of AC electrokinetic-driven flow in a circular microchannel under an imposed wall heat flux. To the author's knowledge, this particular situation has not been explored previously, and is of general interest in the field of thermal electrokinetics. An analytical approach is employed to deal with the energy equation, and then, it is solved by the Green's function method. The velocity profile obtained by [10] is used to perform a parametric study to analyze the associated heat transfer.

2 Problem formulation and analysis

As shown in Fig. 1, two metallic electrodes are situated at each end of the microchannel in which charge separation at the walls has led to the formation of an equilibrium Debye layer. When an electric field, $E_{ext} = E(\omega t)$, is applied along the channel, a body force ($\rho_e E_{ext}$) is exerted on the Debye layer; hence it begins to move and then by viscous drag pulls the charge neutral bulk liquid along. For a fully-developed pure EOF inside a circular microchannel, the equations of potential and velocity fields are [2, 28]:

$$\frac{d^2\psi}{dr^2} + \frac{1}{r}\frac{d\psi}{dr} = -\frac{\rho_e}{\varepsilon} \tag{1}$$

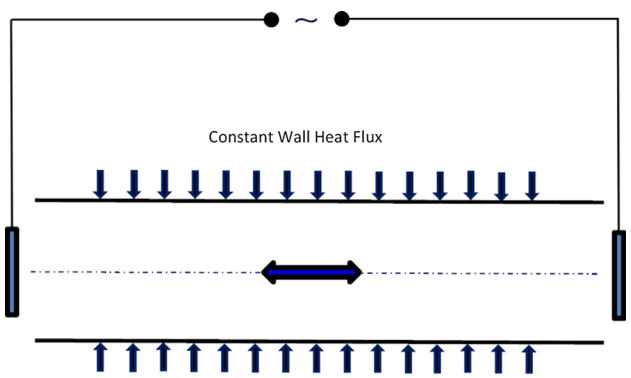

Fig. 1 A schematic of the physical model

$$\rho\frac{\partial V_z}{\partial t}=\mu\left(\frac{\partial^2 V_z}{\partial r^2}+\frac{1}{r}\frac{\partial V_z}{\partial r}\right)-\rho_e E(\omega t) \tag{2}$$

where, ψ is the electrical potential, V_z is the only non-zero velocity component in the channel, ρ and μ are density and viscosity of liquid, respectively, and $E(\omega t)$ is a general time-periodic function with a frequency $\omega = 2\pi f$ that describes the applied electric field strength; the net volume charge density for a symmetric electrolyte ($\mathbb{Z}_- = \mathbb{Z}_+ = \mathbb{Z}$) is $\rho_e = -2\mathbb{Z}en_0 \sinh\left(\frac{\mathbb{Z}e\psi}{k_BT}\right)$. The related boundary conditions are:

$$\begin{cases} r=0 \;:\; \frac{d\psi}{dr}=0 \\ r=\Re \;:\; \psi=\zeta \end{cases} \tag{3}$$

$$\begin{cases} r=0 \;:\; \frac{\partial V_z}{\partial r}=0 \\ r=\Re \;:\; V_z=0 \end{cases} \tag{4}$$

Equation (6), under the condition that the double layer potential Ψ is small, can be linearized by the so-called Debye–Hückel approximation, yielding:

$$\frac{d^2\Psi}{dR^2}+\frac{1}{R}\frac{d\Psi}{dR}=\chi^2\Psi \tag{11}$$

in which, the constant χ has been introduced to denote $\kappa\Re$ (the length scale ratio or the electro-kinetic radius). Solution of (11) subject to the boundary conditions (9) is [10]:

$$\Psi(R)=\frac{\mathrm{Z}}{I_0(\chi)}I_0(\chi R) \tag{12}$$

where, $I_\nu(x)$ is the modified Bessel function of the first kind and order ν.

Solution of Eq. (7), under the Debye–Hückel approximation is [10]:

$$V(R,\theta)=\frac{\chi^2\mathrm{Z}}{\pi I_0(\chi)}\sum_{n=1}^{\infty}\frac{J_0(\beta_n R)\left(\int_0^1 J_0(\beta_n\ell)I_0(\chi\ell)d\ell\right)\left(\beta_n^2\sin(\Omega\theta)-\Omega\cos(\Omega\theta)+\Omega\, e^{-\beta_n^2\theta}\right)}{\left(\beta_n^4+\Omega^2\right)J_1^2(\beta_n)} \tag{13}$$

where, $\Re$ and ζ are the channel radius and the zeta potential of the channel wall, respectively.

Following [10], we consider the dimensionless variables:

$$R=\frac{r}{\Re},\quad \Psi=\frac{\mathbb{Z}e}{k_BT}\psi,\quad \theta=\frac{\mu}{\rho\Re^2}t,\quad \Omega=\frac{\rho\Re^2}{\mu}\omega,$$
$$V=\frac{\mathbb{Z}e\mu}{\varepsilon E_z k_BT}V_z \tag{5}$$

in which, E_z is a constant equivalent to the strength of the applied electric field. The quantity T is considered as a reference characteristic temperature. Equations (1) and (2) can be non-dimensionalized by the above variables as:

$$\frac{d^2\Psi}{dR^2}+\frac{1}{R}\frac{d\Psi}{dR}=(\kappa\Re)^2\sinh(\Psi) \tag{6}$$

$$\frac{\partial V}{\partial\theta}=\frac{\partial^2 V}{\partial R^2}+\frac{1}{R}\frac{\partial V}{\partial R}+(\kappa\Re)^2\sinh(\Psi)F(\Omega\theta) \tag{7}$$

where, $F(\Omega\theta)$ is a general periodic function of unit magnitude such that $E(\Omega\theta) = E_z F(\Omega\theta)$. κ is the Debye–Hückel parameter defined as follows:

$$\kappa=\left(\frac{2\mathbb{Z}^2e^2n_0}{\varepsilon k_BT}\right)^{1/2} \tag{8}$$

The boundary conditions (3) and (4) also take the following dimensionless form:

$$\begin{cases} R=0 \;:\; \frac{d\Psi}{dR}=0 \\ R=1 \;:\; \Psi=\mathrm{Z} \end{cases} \tag{9}$$

$$\begin{cases} R=0 \;:\; \frac{\partial V}{\partial R}=0 \\ R=1 \;:\; V=0 \end{cases} \tag{10}$$

for the sine wave $F(\Omega\theta) = \sin(\Omega\theta)$, where, β_n is the nth root of $J_0(\beta) = 0$.

Now, we consider the energy equation with constant thermo-physical properties [3]:

$$\rho c_p\left(\frac{\partial T}{\partial t}+|V_z|\frac{\partial T}{\partial z}\right)=k_{th}\left[\frac{1}{r}\frac{\partial}{\partial r}\left(r\frac{\partial T}{\partial r}\right)+\frac{\partial^2 T}{\partial z^2}\right]+\sigma E^2(\omega t) \tag{14}$$

in which ρ, c_p, k_{th}, and σ are the fluid density, specific heat, thermal conductivity, and electrical conductivity, respectively, and the last term is the volumetric heat generation due to Joule heating. It should be noted that because of oscillatory velocity profiles in the time-periodic EOF, there are not any recognizable upstream and downstream regions; in other words, depending on time, both axial directions (i.e. $z^-$and z^+) represent upstream and downstream properties. Hence, contrary to direct current (DC) electroosmotic flow, the advection term of Eq. (14) is written with respect to the absolute value of the axial velocity; in fact, as we will prove later, the axial temperature variation is only time-dependent for the fully-developed condition in a long channel. The classical definition of a thermally-fully-developed region requires that:

$$\frac{\partial}{\partial z}\left(\frac{T_s-T}{T_s-T_m}\right)=0 \tag{15}$$

where, T_s and T_m are the local wall temperature and the bulk mean fluid temperature, respectively. The bulk mean fluid temperature is determined from:

$$T_m=\frac{1}{V_{|z,m|}A_c}\int_{A_c}|V_z|T\,dA_c \tag{16}$$

in which, $V_{|z,m|}$ and $A_c = \pi \Re^2$ are the mean fluid velocity (based on the absolute values of local velocities across the channel) and cross-sectional area of the channel, respectively. Under an imposed wall heat flux condition, q''_s, after expanding Eq. (15) and solving for $\partial T/\partial z$, we have:

$$\frac{\partial T}{\partial z} = \frac{\partial T_m}{\partial z} \equiv \text{function of time} \tag{17}$$

and thus $\frac{\partial^2 T}{\partial z^2} = 0$. As a result, the energy Eq. (14) is reduced to:

$$\rho c_p \left(\frac{\partial T}{\partial t} + |V_z| \frac{\partial T_m}{\partial z} \right) = k_{th} \left[\frac{1}{r} \frac{\partial}{\partial r} \left(r \frac{\partial T}{\partial r} \right) \right] + \sigma E^2(\omega t) \tag{18}$$

This equation is subject to the following boundary conditions:

$$\frac{\partial T}{\partial r} = 0 \quad \text{at} \quad r = 0 \tag{19a}$$

$$q''_s = k_{th} \frac{\partial T}{\partial r} \quad \text{at} \quad r = \Re \tag{19b}$$

When thermal energy enters into the channel, q''_s is positive, and vice versa. Moreover, if an overall energy balance is carried out on the fluid, the following result will be obtained:

$$\frac{\partial T_m}{\partial z} = \frac{2q''_s + \Re\left[\sigma E^2(\omega t)\right]}{\rho c_p \Re V_{|z,m|}} \tag{20}$$

Then, the energy Eq. (18) is re-written as follows:

$$\frac{\partial T}{\partial t} = \frac{k_{th}}{\rho c_p} \frac{1}{r} \frac{\partial}{\partial r} \left(r \frac{\partial T}{\partial r} \right) + \frac{1}{\rho c_p} \sigma E^2(\omega t) - |V_z| \left\{ \frac{2q''_s + \Re\left[\sigma E^2(\omega t)\right]}{\rho c_p \Re V_{|z,m|}} \right\} \tag{21}$$

With the help of (5) and introducing the dimensionless temperature:

$$\Phi = \frac{T - \bar{T}_s}{\Re q''_s / k_{th}} \tag{22}$$

we obtain the following non-dimensional energy equation:

$$\frac{\partial \Phi}{\partial \theta} = \frac{1}{\mathrm{Pr}} \frac{1}{R} \frac{\partial}{\partial R} \left(R \frac{\partial \Phi}{\partial R} \right) + \underbrace{\frac{1}{\mathrm{Pr}} \left[G_s - (2 + G_s) \frac{|V|}{V_{|m|}} \right]}_{Q(R,\theta)} \tag{23}$$

where, $\mathrm{Pr} = \frac{\nu}{\alpha}$ and $V_{|m|} = 2 \int_0^1 R|V|\,dR$ are the Prandtl number and dimensionless absolute mean fluid velocity, respectively. It is noted that the averaged surface temperature quantity over one period $\bar{T}_s = \left(1/2\pi\right) \int_0^{2\pi} T_s d(\Omega\theta)$ is constant. The non-dimensional parameter G_s indicates the relative importance of Joule heating and the surface heat flux (the thermal scale ratio), and is defined as:

$$G_s = \frac{\Re}{q''_s} \left[\sigma E_z^2 F^2(\Omega\theta) \right] \tag{24}$$

This parameter is generally time-dependent, and in the case of constant wall heat flux ($q''_s = Q_0$), it can be expressed as $G_s = Q_{0s} F^2(\Omega\theta)$, in which, Q_{0s} is a constant. It should be noted that G_s can be either positive (if $Q_0 > 0$, i.e. surface heating) or negative (if $Q_0 < 0$, i.e. surface cooling).

The thermal boundary conditions (19) in dimensionless form are:

$$\frac{\partial \Phi}{\partial R} = 0 \quad \text{at} \quad R = 0 \tag{25a}$$

$$\frac{\partial \Phi}{\partial R} = 1 \quad \text{at} \quad R = 1 \tag{25b}$$

The dimensionless mean fluid temperature is determined as:

$$\Phi_m = \frac{2}{V_{|m|}} \int_0^1 R|V|\Phi\, dR \tag{26}$$

The fully-developed Nusselt number may be expressed generally as:

$$Nu_\theta = \frac{-2}{\Phi_m} \tag{27}$$

It is noted that the above Nusselt number is time-dependent. The fully-developed mean-time Nusselt number (evaluated at one period) is defined as:

$$Nu = \frac{1}{2\pi} \int_0^{2\pi} Nu_\theta d(\Omega\theta) \tag{28}$$

3 Solution procedure

The non-dimensional energy Eq. (23) subject to the boundary conditions (25) is now solved by using a Green's function approach. The Green's function satisfies:

$$\frac{\partial g}{\partial \theta} - \frac{1}{\mathrm{Pr}} \frac{1}{R} \frac{\partial}{\partial R} \left(R \frac{\partial g}{\partial R} \right) = \frac{\delta(R - \ell)\delta(\theta - \tau)}{2\pi R} \tag{29}$$

subject to the following homogeneous boundary conditions:

$$\left\{ \begin{array}{l} \lim_{R \to 0} \left| g\left(R, \theta : \ell, \tau\right) \right| < \infty \\ \frac{\partial g}{\partial R}\left(1, \theta : \ell, \tau\right) = 0 \end{array} \right\} \quad 0 < R, \ell < 1 \quad \& \quad 0 < \theta, \tau \tag{30}$$

and the initial condition $g(R, 0{:}1, \tau) = 0$. $\delta(x)$ is the Dirac delta function.

We begin by taking the Laplace transform (29):

$$\frac{1}{R}\frac{d}{dR}\left(R\frac{dG}{dR}\right) - \mathrm{Pr}\, s\, G = -\frac{\mathrm{Pr}\, e^{-s\tau}}{2\pi R}\delta(R-\ell) \tag{31}$$

Next, $\delta(R-1)/R$ is expressed as the Fourier–Bessel expansion:

$$\frac{\delta(R-\ell)}{2\pi R} = \sum_{n=0}^{\infty} A_n J_0(\lambda_n R) \tag{32}$$

where, λ_n is the nth root of $J_1(\lambda) = 0$, and:

$$\begin{aligned} A_n &= \frac{2}{J_0^2(\lambda_n) + J_1^2(\lambda_n)} \int_0^1 \frac{\delta(R-\ell)}{2\pi R} J_0(\lambda_n R) R\, dR \\ &= \frac{J_0(\lambda_n \ell)}{\pi\left[J_0^2(\lambda_n) + J_1^2(\lambda_n)\right]} \end{aligned} \tag{33}$$

so that Eq. (31) is re-written as:

$$\frac{1}{R}\frac{d}{dR}\left(R\frac{dG}{dR}\right) - \mathrm{Pr}\, s\, G = -\frac{\mathrm{Pr}\, e^{-s\tau}}{\pi} \sum_{n=0}^{\infty} \frac{J_0(\lambda_n \ell) J_0(\lambda_n R)}{J_0^2(\lambda_n) + J_1^2(\lambda_n)} \tag{34}$$

The solution to (34) is:

$$G\left(R, s{:}\ell, \tau\right) = \frac{e^{-s\tau}}{\pi} \sum_{n=0}^{\infty} \frac{J_0(\lambda_n \ell) J_0(\lambda_n R)}{\left(s + \frac{\lambda_n^2}{\mathrm{Pr}}\right)\left[J_0^2(\lambda_n) + J_1^2(\lambda_n)\right]} \tag{35}$$

Taking the inverse of (35) and applying the second shifting theorem:

$$g\left(R, \theta{:}\ell, \tau\right) = \frac{H(\theta-\tau)}{\pi} \sum_{n=0}^{\infty} \frac{J_0(\lambda_n \ell) J_0(\lambda_n R)}{J_0^2(\lambda_n) + J_1^2(\lambda_n)} e^{\frac{-\lambda_n^2}{\mathrm{Pr}}(\theta-\tau)} \tag{36}$$

in which, $H(x)$ is the Heaviside step function.

So the dimensionless temperature profile is calculated by the following simplified formula:

$$\begin{aligned} \Phi(R,\theta) = &\int_0^{\theta}\int_0^1 g\left(R, \theta{:}\ell, \tau\right) Q(\ell, \tau) d\ell\, d\tau \\ &+ \frac{1}{\mathrm{Pr}} \int_0^{\theta} g\left(R, \theta{:}1, \tau\right) d\tau \end{aligned} \tag{37}$$

where, $Q(1, \tau)$ is defined in Eq. (23). Once the dimensionless temperature distribution is determined, the dimensionless mean fluid temperature and the fully-developed Nusselt number can be evaluated from Eqs. (26) and (27), respectively. The method of Simpson quadrature has been used to perform the required integrations. A spatial-step of $\Delta R = 0.0001$ and a time-step of $\Delta\theta = (\pi/400)/\Omega$ are found to be satisfactory in obtaining sufficient accuracy within a tolerance of 10^{-6} in nearly all cases.

Green's function is generally introduced as a solution due to a concentrated source at a position (within the domain) acting instantaneously only at one moment. It is noteworthy that the Green's function approach is primarily utilized to solve non-homogeneous problems. Actually, there is one function for each problem, called the Green's function, which can be used to describe the influence of all kinds of non-homogeneity (either in equation or in boundary conditions). This method includes the following basic steps: (1) Write the original differential equation subject to its boundary conditions (both may be non-homogeneous); (2) Write the governing equation of the related Green's function (using the definition of the Dirac delta function) subject to the corresponding homogeneous boundary conditions; (3) Solve the Green's function problem; (4) The relationship between the Green's function and the solution of the non-homogeneous original problem is established using the appropriate Green's formula.

4 Results and discussion

In this analytical description of AC electroosmotic flow and associated heat transfer in a circular microchannel, the governing parameters are Ω (the ratio of the diffusion time scale to the period of the applied electric field), χ (the ratio of half channel diameter to Debye length), and G_s (the ratio of Joule heating to surface heat flux). A systematic study is performed to examine the influence of the governing parameters on the time-periodic EOF heat transfer in a circular microchannel. Investigation of the source term of Eq. (23) reveals that the temperature field repeats itself at each half-period; hence, only the results of a half-period ($0 < \Omega\theta \le \pi$) of the sine wave are presented. The effect of the constant wall heat flux condition (equivalent to time-periodic thermal scale ratio) on the fluid flow thermal behavior will also been considered for a selective value of the Prandtl number ($\mathrm{Pr} = 100$).

Figure 2 shows the steady-state time-periodic velocity profiles for a half-period of the sine wave [obtained from Eq. (13)] in a circular microchannel for two frequencies $\Omega = 30$ and $\Omega = 300$, and two length scale ratios $\chi = 300$ and $\chi = 600$. These two Ω values correspond to frequencies of 500 Hz and 5 kHz in a 100 μm channel. Two values of double layer thickness, i.e. $\kappa = 6 \times 10^6\ \mathrm{m}^{-1}$ and $\kappa = 1.2 \times 10^7\ \mathrm{m}^{-1}$, are also examined; a uniform surface potential of $\zeta = 12.5$ mv is used (within the bounds imposed by the Debye–Hückel linearization). In the case of

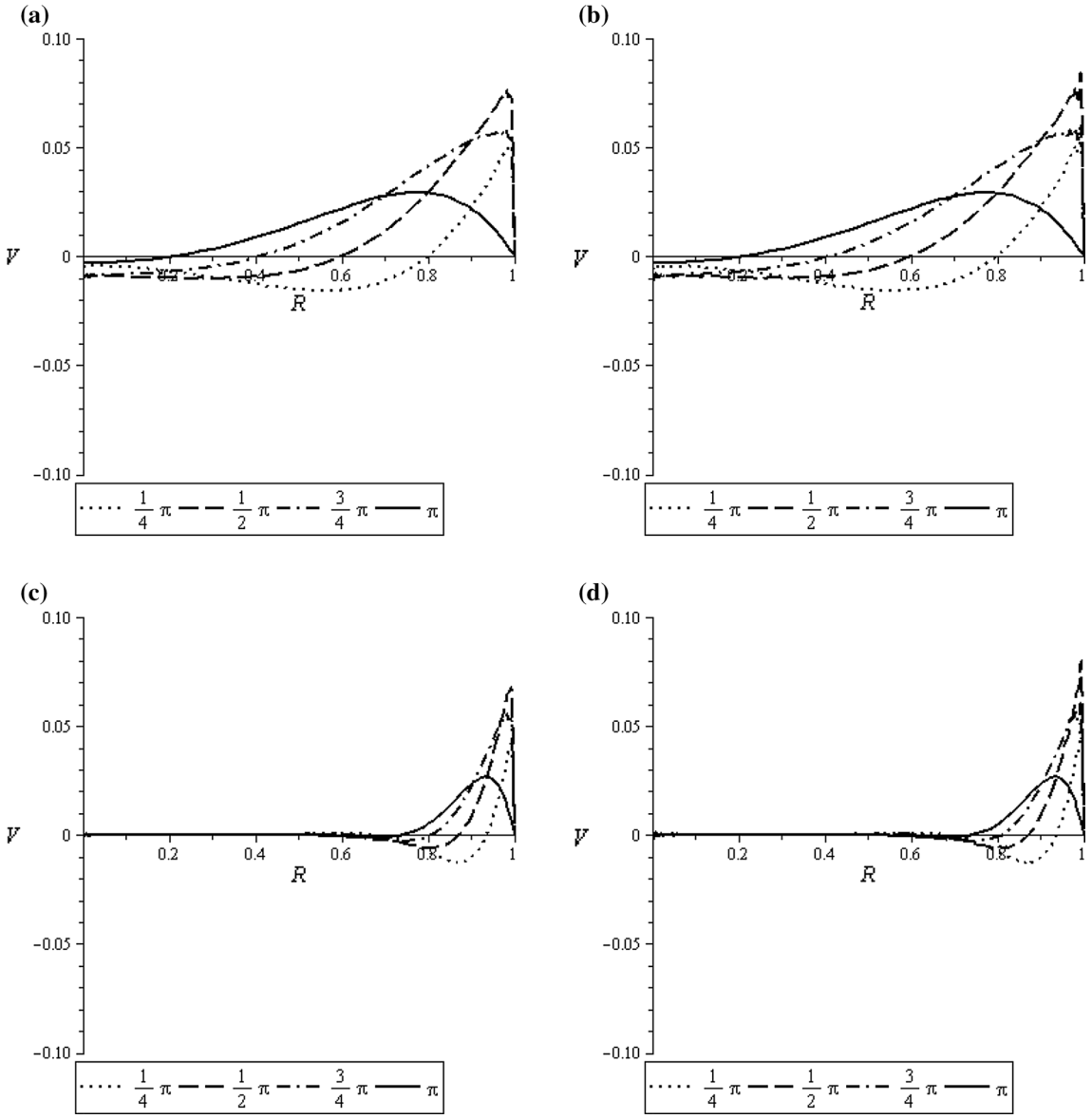

Fig. 2 Steady-state time periodic non-dimensional velocity profiles for a half-period ($0 < \Omega\theta \leq \pi$) of the sine wave and **a** $\Omega = 30$, $\chi = 300$, **b** $\Omega = 30$, $\chi = 600$, **c** $\Omega = 300$, $\chi = 300$, **d** $\Omega = 300$, $\chi = 600$

high Ω value, there is insufficient time for fluid momentum to diffuse far into the bulk flow, and thus, while the fluid within the EDL oscillates rapidly, the bulk fluid remains almost stationary.

The dimensionless temperature profiles in the case of constant wall heat flux with $Q_{0s} = 2$ (surface heating) are shown in Fig. 3 for various values of Ω and χ. The bulk fluid temperature oscillates in a certain range at one period. In the case of surface heating and for low values of the frequency (Fig. 3a, b), the negative values of dimensionless temperature are observed; according to Eq. (22), it means $T < T_s$. In fact, the bulk fluid has sufficient time to transport the resultant heating (combination of Joule heating and wall heat flux) in the axial direction. However, for sufficiently high values of the frequency (Fig. 3c, d), positive values of dimensionless temperature are temporarily illustrated in the middle part of the channel. In this case, as may be seen in Fig. 2c, d, the relatively broad range of the cross-sectional area is almost immobile, and only the region near the channel wall oscillates rapidly. Hence, the temperature values of this central area are further enhanced at some times, since the influence of the advection mechanism on that area is weakened.

The effect of Q_{0s} on the dimensionless temperature distribution at $\chi = 600$ and $\Omega = 30$ is illustrated in Fig. 4. Recall that Q_{0s} is positive for surface heating ($q_s'' > 0$)

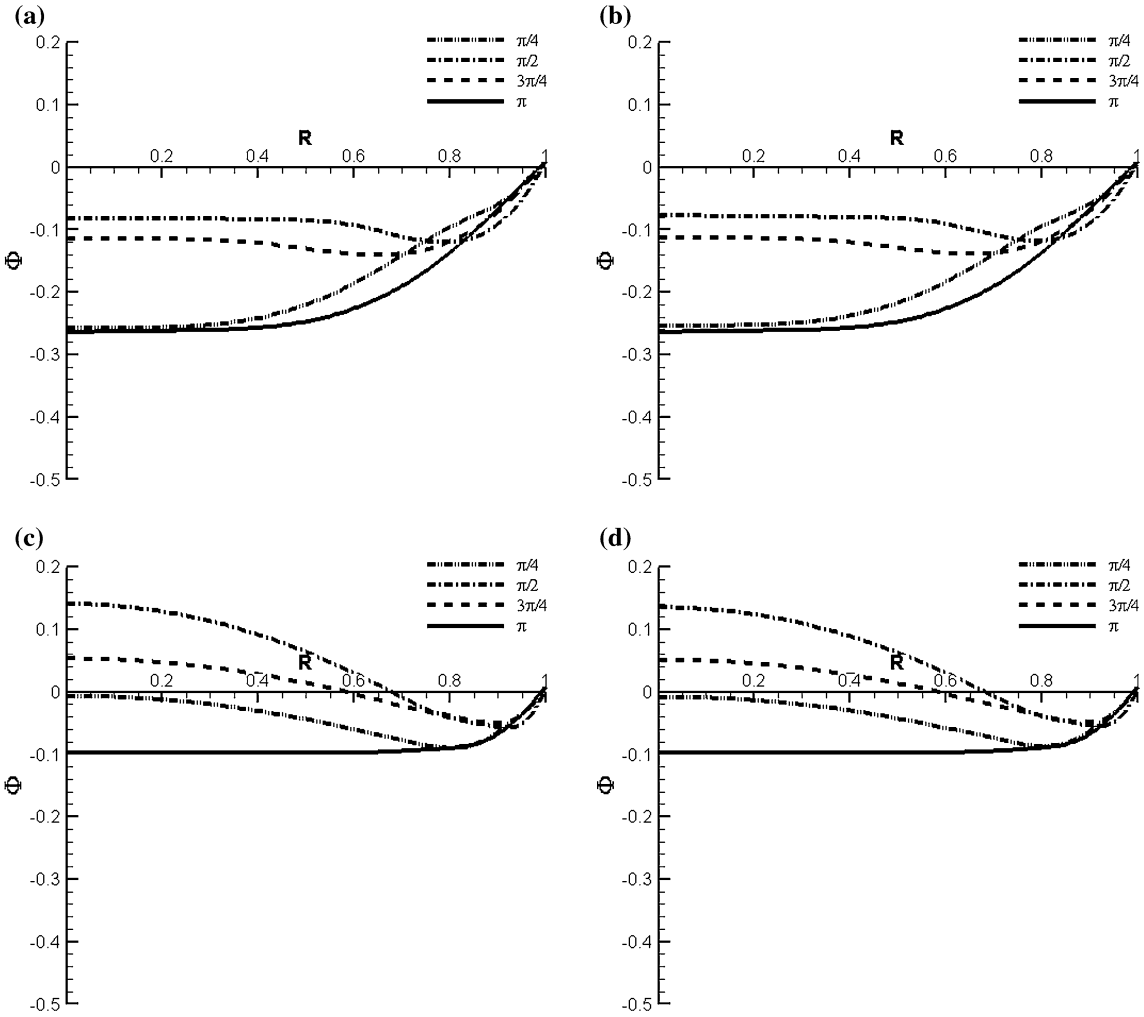

Fig. 3 Steady-state time periodic non-dimensional temperature profiles for a half-period ($0 < \Omega\theta \leq \pi$) of the sine wave with $Q_{0s} = 2$ at **a** $\Omega = 30$, $\chi = 300$, **b** $\Omega = 30$, $\chi = 600$, **c** $\Omega = 300$, $\chi = 300$ and **d** $\Omega = 300$, $\chi = 600$

and negative for surface cooling ($q_s'' < 0$). It is clear that increasing the value of Q_{0s} results in increasing the dimensionless temperature for $\Omega = 30$; meanwhile, an increase in the absolute value of Q_{0s} leads to broaden the temperature distribution at one period. As the dimensionless temperature distribution has negative values, the bulk fluid temperature is higher than the wall temperature for the cooling condition; the reverse is true for the heating state [it can also be concluded from Eq. (22)]. The interesting case of constant wall temperature occurs at $\Omega\theta = \pi/2$ with $Q_{0s} = -2$ (Fig. 4b), in which $G_s = -2$ and according to Eq. (23), the temperature profile does not depend on the velocity variations (it is independent of Ω and χ). In fact, this instantaneous unique form of a function of Φ corresponds to the condition in which all the energy produced by Joule heating is dissipated at the channel wall, yielding $q_s'' < 0$ (surface cooling); this special case is one for which $\partial T_m/\partial z = 0$ and thus $\partial T_s/\partial z = 0$ for thermally fully-developed flow in a microchannel with constant wall heat flux.

Figure 5 demonstrates the dimensionless temperature profiles at $\chi = 600$ and $\Omega = 300$ for various values of Q_{0s}. Increasing the dimensionless frequency causes two distinct events: broadening the dimensionless temperature distribution for the surface cooling state at one period (compare Figs. 4a, 5a), and locally illustrating the positive dimensionless temperature profiles for the surface heating state at some moments. It is noted that both Joule heating and velocity field are periodic functions; hence, the resultant leads to widen out the temperature field at one period as the frequency is increased. Since the bulk fluid is almost stationary at sufficiently large Ω, its dimensionless temperature distribution takes positive values in the case of surface heating (the bulk fluid temperature becomes greater than the surface temperature); in fact, the advection mechanism

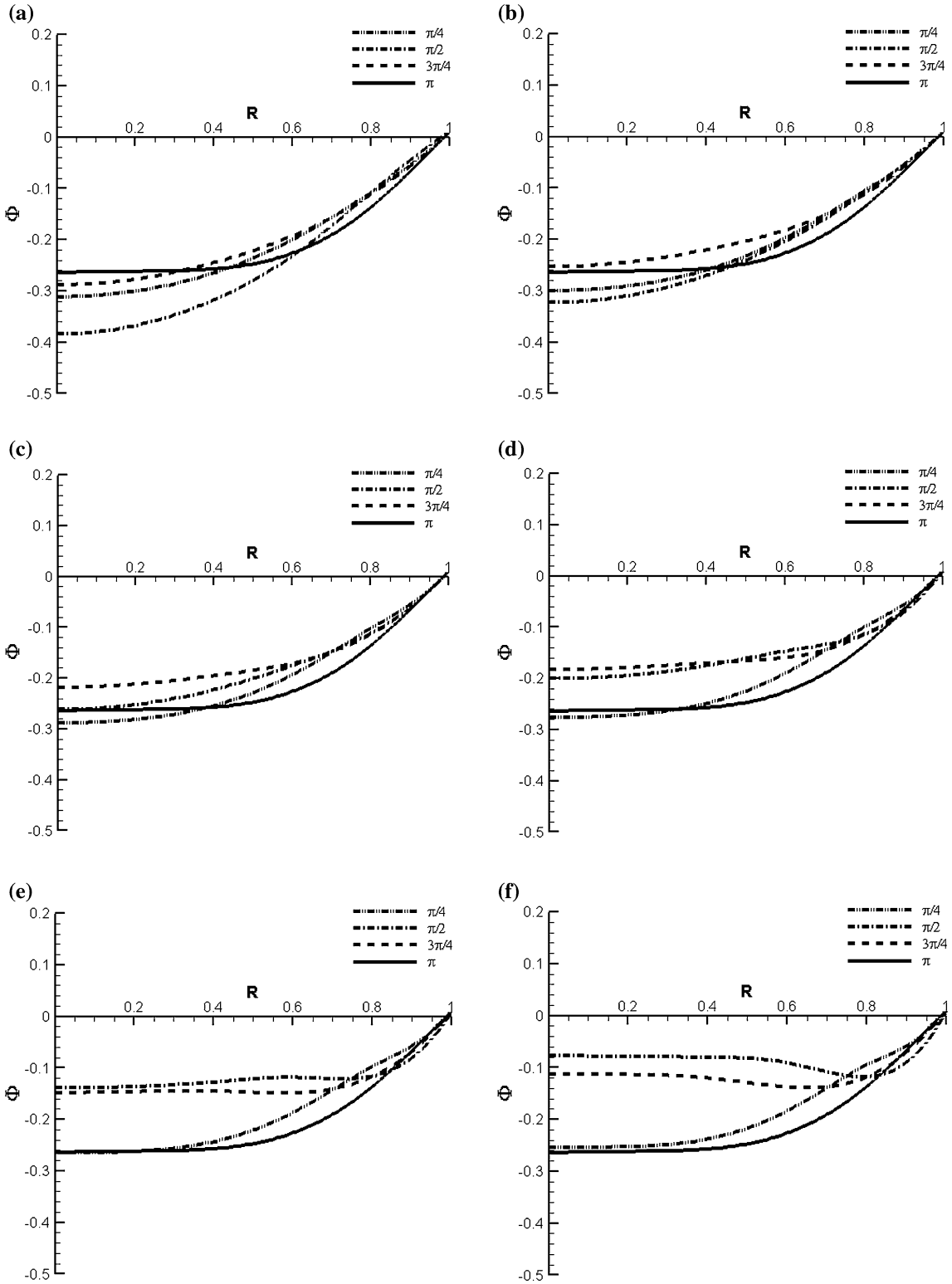

Fig. 4 Steady-state time periodic non-dimensional temperature profiles for a half-period ($0 < \Omega\theta \leq \pi$) of the sine wave with $\chi = 600$ and $\Omega = 30$ at **a** $Q_{0s} = -3$, **b** $Q_{0s} = -2$, **c** $Q_{0s} = -1$, **d** $Q_{0s} = 0$, **e** $Q_{0s} = 1$ and **f** $Q_{0s} = 2$

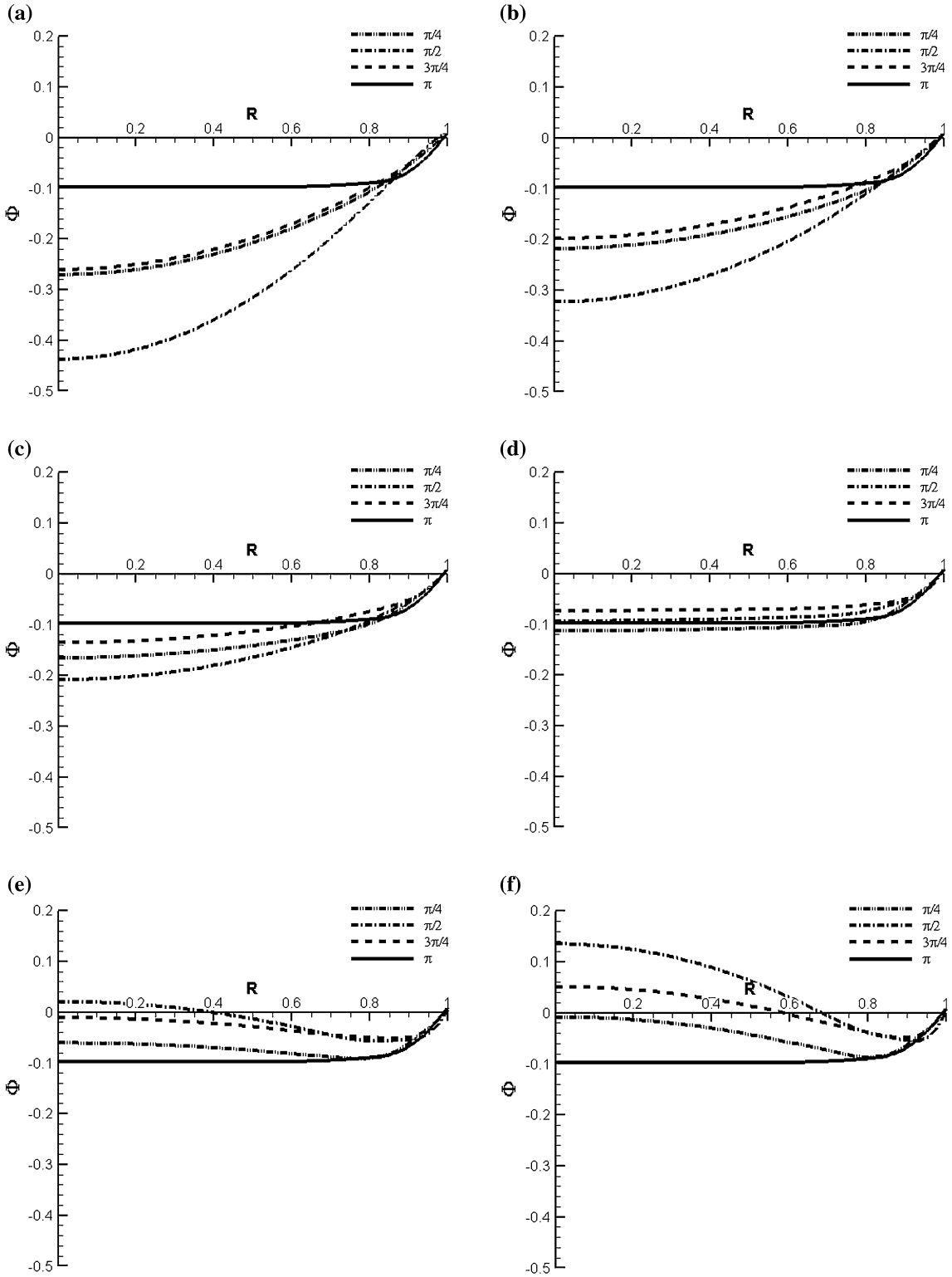

Fig. 5 Steady-state time periodic non-dimensional temperature profiles for a half-period ($0 < \Omega\theta \leq \pi$) of the sine wave with $\chi = 600$ and $\Omega = 300$ at **a** $Q_{0s} = -3$, **b** $Q_{0s} = -2$, **c** $Q_{0s} = -1$, **d** $Q_{0s} = 0$, **e** $Q_{0s} = 1$ and **f** $Q_{0s} = 2$

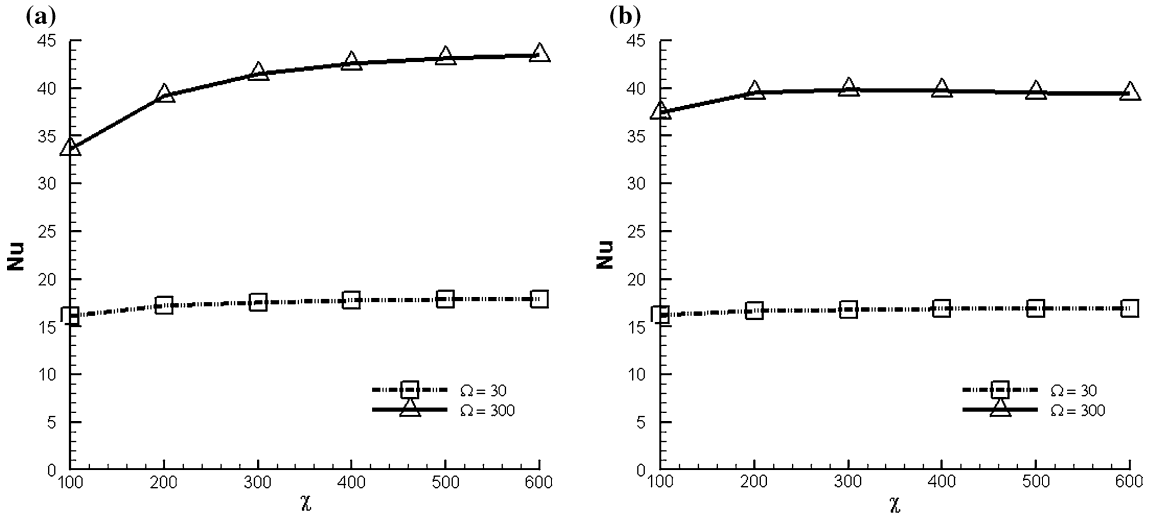

Fig. 6 Variations of quasi-steady-state mean-time Nusselt number with χ for the sine wave and in two cases of **a** $Q_{0s} = 2$ (surface heating) and **b** $Q_{0s} = -3$ (surface cooling)

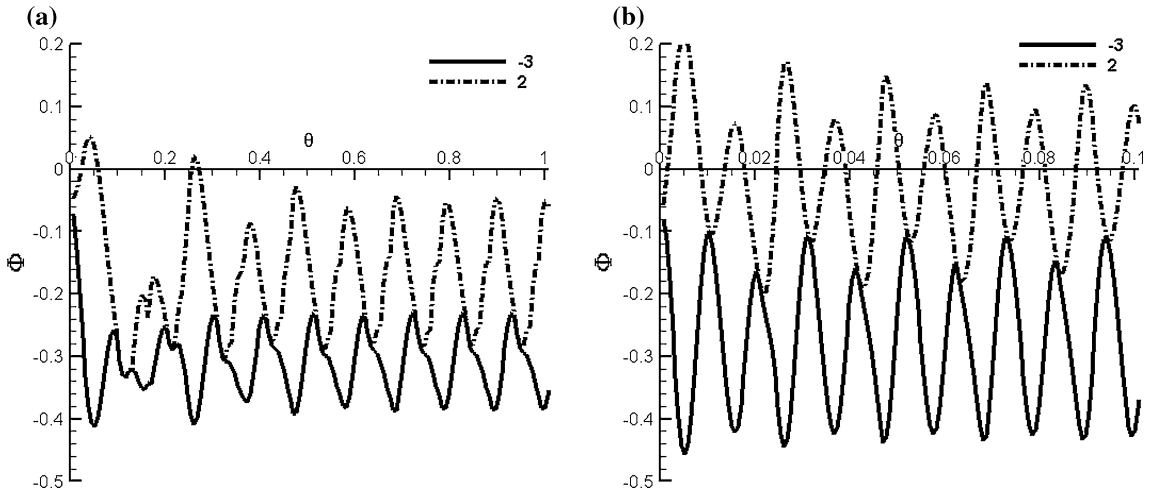

Fig. 7 Transient stage non-dimensional temperature at the channel midpoint for the sine wave at $\chi = 600$, and two various values of Q_{0s} and **a** $\Omega = 30$ and **b** $\Omega = 300$

is weak and there is not enough time to sweep heat into downstream. It is obvious from Figs. 4 and 5 when $G_s = 0$ (either $Q_{0s} = 0$ or $\Omega\theta = 0$), effect of Joule heating vanishes.

Figure 6 plots the quasi-steady-state mean-time Nusselt number as a function of the length scale ratio (χ) for two Ω values and the surface cooling and heating conditions. Clearly, the fully-developed mean-time Nusselt number increases with frequency. Nusselt number generally approaches a specific value as $\chi \to \infty$; in the case of surface heating with $\Omega = 30$ and $\Omega = 300$, it would be nearly 18 and 45, respectively, and in the case of surface cooling with $\Omega = 30$ and $\Omega = 300$, it would be nearly 17 and 40, respectively.

The effects of frequency and surface cooling and heating on the transient response of the channel mid-point (at $R = 0$) are shown in Fig. 7 (here, the channel mid-point is selected as a representative point of the bulk fluid). Obviously, the mid-point dimensionless temperature corresponding to the surface cooling state is more negative than the relevant temperature corresponding to the surface heating state. In other words, in the presence of Joule heating, surface cooling decreases the wall temperature, while surface heating increases it; hence, the temperature difference of the channel wall and mid-point in the case of surface cooling would be greater than that of the surface heating state. Comparison of Fig. 7a, b shows that the

transient-stage mid-point temperature amplitude increases with frequency. Also, the curve related to surface heating is shifted upward and has positive peaks, which is consistent with Fig. 5f.

5 Concluding remarks

In this study, the thermal transport characteristics of time-periodic EOF in a circular microchannel have been investigated. The problem was found to be governed by three parameters, namely, the dimensionless frequency, the length scale ratio, and the thermal scale ratio. Inside the fluid is the Joule heating (always with a positive sign), and a constant surface heat flux is imposed to the channel wall. Therefore, the thermal scale ratio may be positive (surface heating) or negative (surface cooling), depending on the sign of wall heat flux. In the case of constant wall heat flux, the thermal scale ratio is time-dependent ($G_s = Q_{0s}F^2(\Omega\theta)$) whose sign is determined by Q_{0s}. The resultant internal heating (or cooling) of the bulk fluid is transferred in the axial direction by the advection mechanism. The solutions are obtained for a wide range of the governing parameters. The main results of the present work can be summarized as follows:

1. For each period of the velocity field, there are two similar half-period of the temperature field; i.e. the temperature field repeats itself for each half-period.
2. Increasing the electrokinetic radius leads to decrease the temperature difference between the wall and the fluid for the case of surface heating.
3. Frequency has a strong influence on the thermal behavior of the flow field. Generally, when the frequency is small, the complete flow field has sufficient time to transfer the resultant heating (Joule heating as well as wall heat flux) in the axial direction. However, at high frequencies, the middle portion of the flow field is almost stationary, and does not carry heat along the channel (the near-wall section will mainly transport the resultant heating in the axial direction); in fact, the influence of the advection mechanism on the central area is weakened.
4. For relatively high frequencies, and at each individual moment, there is one cylindrical surface in the channel whose temperature equals the wall temperature; i.e. a cylindrical surface with zero radial heat flux.
5. In the case of constant wall heat flux and for the sinusoidal waveform, there is one particular moment, i.e. at $\theta = \pi$, whose dimensionless temperature is independent of the value of wall heat flux.
6. The temperature profile has a unique form of Φ for $G_s = -2$ regardless of Ω and χ, which is the asymptotic solution of a constant wall temperature boundary condition (for which $\partial T/\partial z = 0$); this special case corresponds to the surface cooling state.
7. The quasi-steady-state mean-time Nusselt number generally approaches a specific value as $\chi \to \infty$; its value depends upon the frequency as well as the type of wall heat flux.
8. Joule heating exists in the electroosmotic flow; now, if the channel wall is influenced by surface cooling, the wall temperature decreases, while if surface heating is applied, the channel wall temperature increases. Therefore, the temperature difference of the channel wall and mid-point in the case of surface cooling would be greater than that of the surface heating state.
9. Increasing the dimensionless frequency (larger channel size, smaller kinematic viscosity, or greater frequency) results in broadening the temperature field at one moment; at sufficiently high values of Ω, the bulk fluid temperature may become greater than the wall temperature at some moments.
10. The effects of frequency on the transient-stage dimensionless temperature of the mid-point are to enhance the oscillation amplitude as well as an upward movement in the whole curve, especially in the surface heating condition in which positive values of Φ are also observed.
11. The steady-state time-periodic dimensionless temperature is independent of Prandtl number.

References

1. Bruus H (2008) Theoretical microfluidics. Oxford University Press Inc., New York
2. Tabeling P (2005) Introduction to microfluidics. Oxford University Press, New York
3. Hardt S, Schonfeld F (2007) Microfluidic technologies for miniaturized analysis systems. Springer, New York
4. Arulanandam S, Li D (2000) Liquid transport in rectangular microchannels by electro-osmotic pumping. Colloids Surf A 161:89–102
5. Erickson D, Li D (2003) Analysis of AC electroosmotic flows in a rectangular microchannel. Langmuir 19:5421–5430
6. Kang YJ, Yang C, Huang XY (2002) Dynamic aspects of electroosmotic flow in a cylindrical microcapillary. Int J Eng Sci 40:2203–2221
7. Tang GH, Li XF, Tao WQ (2010) Microannular electro-osmotic flow with the axisymmetric lattice Boltzmann method. J Appl Phys 108(11):114903
8. Wang M, Kang Q (2010) Modeling elctrokinetic flows in microchannels using coupled lattice Boltzmann methods. J Comput Phys 229:728–744
9. Xuan XC, Li D (2005) Electroosmotic flow in microchannels with arbitrary geometry and arbitrary distribution of wall charge. J Colloid Interface Sci 289:291–303
10. Moghadam AJ (2012) An exact solution of AC electro-kinetic-driven flow in a circular micro-channel. Eur J Mech B/Fluids 34:91–96

11. Oddy MH, Santiago JG, Mikkelsen JC (2001) Electrokinetic instability micromixing. Anal Chem 73:5822–5832
12. Dutta P, Beskok A (2001) Analytical solution of time periodic electroosmotic flows: analogies to stokes second problem. Anal Chem 73:5097–5102
13. Soderman O, Jonsson B (1996) Electro-osmosis: velocity profiles in different geometries with both temporal and spatial resolution. J Chem Phys 105:10300–10311
14. Green NG, Ramos A, Gonzalez A, Morgan H, Castellanos A (2000) Fluid flow induced by non-uniform AC electric fields in electrolytes on microelectrodes I: experimental measurements. Phys Rev E 61:4011–4018
15. Gonzalez A, Ramos A, Green NG, Castellanos A, Morgan H (2000) Fluid flow induced by non-uniform AC electric fields in electrolytes on microelectrodes II: A linear double layer analysis. Phys Rev E 61:4019–4028
16. Brown ABD, Smith CG, Rennie AR (2002) Pumping of water with an AC electric field applied to asymmetric pairs of microelectrodes. Phys Rev E 63:016305
17. Studer V, Pepin A, Chen Y, Ajdari A (2002) Fabrication of microfluidic devices for AC electrokinetic fluid pumping. Microelectron Eng 61–62:915–920
18. Moghadam AJ (2013) Exact solution of AC electro-osmotic flow in a microannulus. ASME J Fluids Eng 135:091201
19. Moghadam AJ (2014) Effect of periodic excitation on alternating current electroosmotic flow in a microannular channel. Eur J Mech B/Fluids 48:1–12
20. Soong CY, Wang SH (2003) Theoretical analysis of electrokinetic flow and heat transfer in a microchannel under asymmetric boundary conditions. J Colloid Interface Sci 265(1):202–213
21. Yang C, Li D, Masliah JH (1998) Modeling forced liquid convection in rectangular microchannels with electrokinetic effects. Int J Heat Mass Transf 41:4229–4249
22. Maynes D, Webb BW (2003) Fully developed electro-osmotic heat transfer in microchannels. Int J Heat Mass Transf 46:1359–1369
23. Chen C-H (2009) Thermal transport characteristics of mixed pressure and electro-osmotically driven flow in micro- and nonochannels with joule heating. ASME J Heat Transf 131:022401
24. Sadeghi A, Saidi MH (2010) Viscous dissipation effects on thermal transport characteristics of combined pressure and electroosmotically driven flow in microchannels. Int J Heat Mass Transf 53:3782–3791
25. Moghadam AJ (2014) Thermally developing flow induced by electro-osmosis in a circular micro-channel. Arab J Sci Eng 39:1261–1270
26. Maynes D, Webb BW (2004) The effect of viscous dissipation in thermally fully-developed electro-osmotic heat transfer in microchannels. Int J Heat Mass Transf 47:987–999
27. Moghadam AJ (2013) Electrokinetic-driven flow and heat transfer of a non-newtonian fluid in a circular microchannel. ASME J Heat Transf 135:021705
28. Nguyen NT, Wereley ST (2006) Fundamentals and Applications of Microfluidics. ARTECH HOUSE, Boston